Evaluation of Materials and Surfaces for Lunar Regolith Adherence Characterization (RAC) payload samples

Authors

Lopamudra Das[1], Christopher J. Wohl[2], Keith L. Gordon[2], Jin Ho Kang[1], Valerie L. Wiesner[2], Glen C. King[2], Samuel J. A. Hocker[2], and Sang H. Choi[2]

[1]National Institute of Aerospace, 100 Exploration Way, Hampton VA-23666
[2]NASA Langley Research Center, Hampton VA-23681

Abstract

As the quest for long term lunar exploration and habitation comes closer to reality, widespread efforts are ongoing to effectively mitigate lunar dust surface contamination and infiltration. This dust is hazardous to humans and tends to adhere tenaciously to all exposed surfaces, causing performance issues and ultimately failure. While several active and passive technologies have been developed to address this challenge, assessing the performance of these technologies in the actual lunar environment is extremely important. The regolith adherence characterization (RAC) experiment payload provides an important opportunity for this evaluation. The RAC payload is designed by Alpha Space for the National Aeronautics and Space Administration (NASA) and scheduled to be flown to the moon in 2023 on the Firefly Aerospace Blue Ghost lander. As there were a limited number of slots available for materials to be chosen for this mission, it was critical to make an informed selection. Two polymers, a carbon fiber reinforced composite and a metal alloy were chosen to be a diverse selection of structural materials from NASA Langley Research Center. Each material was topographically modified using laser ablation patterning. This article briefly describes the selection and testing procedure and some of the results obtained for the passive dust mitigating materials and surfaces selected for this lunar surface experiment.

Introduction

To enable long term and sustained lunar exploration missions, the topic of lunar dust mitigation remains one of significant importance. Lunar dust poses a huge challenge, it consists of porous jagged particles less than 60 µm in size that are abrasive, chemically reactive, electrostatically and sometimes magnetically charged [1]. These particles are mostly silicates in composition, strongly adhere to any exposed surfaces and cause material degradation and failure. Some examples where dust mitigation is essential include spacesuits, optical surfaces, thermal surfaces, electronics and moving mechanical parts. Research is ongoing to find ways of active and passive dust adhesion mitigation strategies on different material surfaces [2–4].

In this study, passive dust adhesion mitigation by material surface modification using laser patterning was explored. The passive method is advantageous in that it does not require any external energy source. It can be used in conjunction with the active methods, such as electrodynamic dust lofting techniques, to provide greater mitigation. The material samples

chosen were characterized by a custom designed dust adhesion testing system, as well as optical microscopy, contact angle goniometry, contact profilometry and scanning electron microscopy (SEM) measurements. Based on these results, the informed selection of the polymeric, carbon fiber reinforced composite and metallic materials with specific patterned surfaces to be flown to the moon for further evaluation is discussed.

Since it is not possible to simulate with perfect fidelity all the lunar environmental conditions on Earth, the commercial lunar payload services (CLPS) missions provide an excellent opportunity to conduct some experiments on the moon for further testing and validation. The selected material test samples on the Regolith Adherence Characterization (RAC) payload (being developed by Alpha Space Test and Research Alliance, LLC) will be mounted to a sample carrier disc and exposed during transit, lunar landing conditions and on the lunar surface to test for dust accumulation using a charge-coupled device (CCD) camera. Those results, when available, will help in evaluating how the selected materials perform in the actual lunar environment relative to that under terrestrial laboratory conditions. At the time this paper was written, the Firefly Aerospace Blue Ghost Lander was selected to deliver the RAC payload to the lunar surface in 2023.

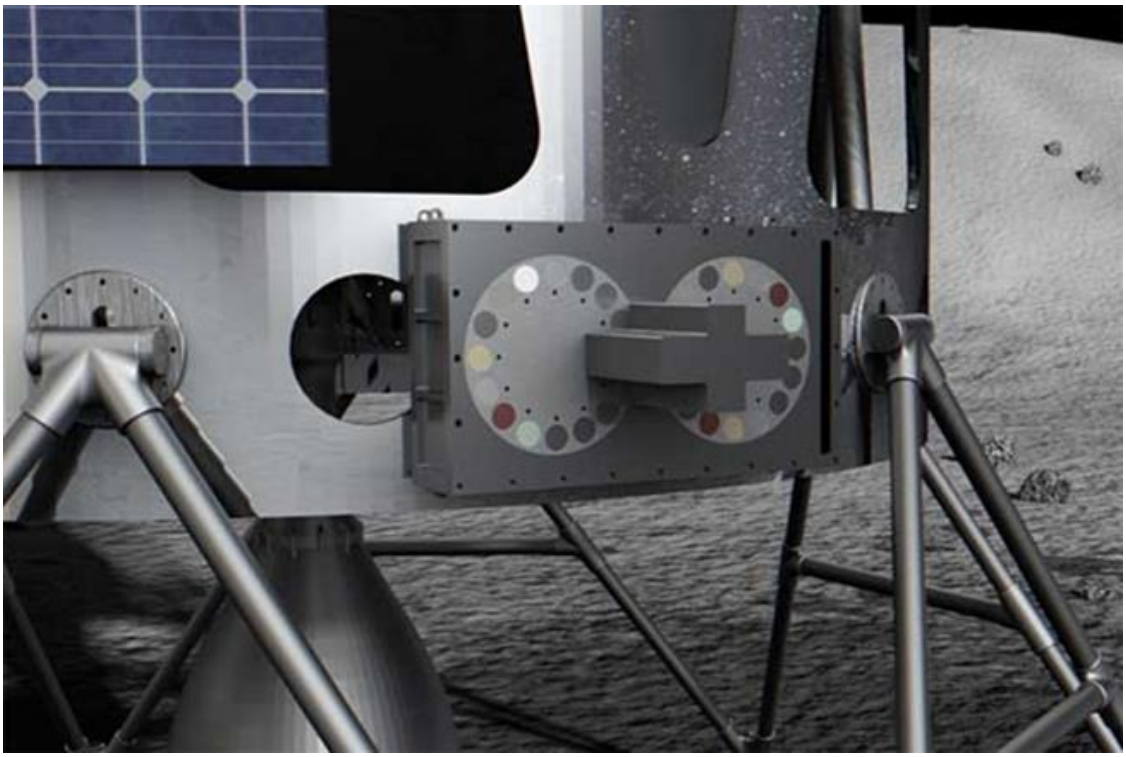

Figure 1. Schematic of the Regolith Adherence Characterization (RAC) payload being provided by Alpha Space Test and Research Alliance, LLC. Image credit: Alpha Space Test and Research Alliance, LLC.

Materials selection for dust adhesion evaluation

The lunar environment is very different from that on Earth, with extreme temperatures ranging from -178˚C to + 123˚C, ultra-high vacuum, reduced gravity, exposure to solar radiation, meteoroid impacts, and electrostatic dust levitation. The materials selected for different applications thus must be stable and durable in that environment. To this end, a range of materials were selected for inclusion in the RAC experiment payload to address needs for a broad application space. The materials described here (Table 1) are those developed at NASA Langley Research Center and are a subset of all the materials to be integrated into the RAC experiment payload.

Table 1. Materials evaluated for inclusion in the RAC experiment payload at NASA Langley Research Center.

Material	Primary Application
Kapton® HN (Dupont™)	Extensive space heritage, excellent thermal stability, chemical resistance, dielectric properties, radiation resistance
Teflon™ FEP (Fluorinated Ethylene Propylene)	Extensive space heritage, excellent thermal stability, low energy surface, chemical resistance, UV stability, dielectric properties
Low Creep/Low Relaxation (LCLR) bismaleimide (BMI) Composite	Use in deployable structures, excellent mechanical and thermal properties
Titanium Alloy (Ti-6Al-4V)	Extensive space heritage as a material in primary structures.

Previous studies have indicated that topographical modification via laser ablation patterning can improve the dust adhesion mitigation properties of material surfaces [5]. In this direct write lithographic technique, micrometer-scaled topographies can be readily generated. Hierarchical topographies, i.e., topographies with features on multiple length scales, are often cited as beneficial for mitigation of contaminant adhesion and, for some of the materials discussed in this work, laser ablation resulted in generation of periodic hierarchical topographies. In all the selected materials, surface topographies were created by laser ablation patterning as will be described below. Pristine and laser ablation patterned surfaces were evaluated for dust adhesion mitigation in support of inclusion in the RAC payload.

Experimental

Commercially available thin films of Teflon™ FEP (508 µm thick) and Dupont™ Kapton® HN (127 µm thick) were obtained from CS Hyde Company, Illinois, U.S. The composite material was generated in the lab, and the titanium alloy samples were obtained from in-house material that was polished by machine lapping with abrasives down to 9 µm in size and cut to the required dimensions using a waterjet machine. For the topographically modified samples, laser patterning was done using a Ekspla, Atlantic 20 Nd:YVO_4 laser at 12.2 W power with a fundamental wavelength of 1064 nm and 10 ps pulse rate. Laser ablation parameters for each

material are shown in Table 2. A crosshatch pattern was created on each sample at a line speed of 76.2 cm/s.

Scanning electron microscopy (SEM) images of each sample surface were taken after laser ablation patterning with a Hitachi S5200 SEM at an acceleration voltage of 10 kV and 25 kV for polymeric and metallic samples, respectively. Optical microscopy images of the sample surfaces at 10x, 20x and 50x magnification were also obtained using a Leica DFC 450 Optical microscope. Images were taken with brightfield illumination, as well as with cross-polarized illumination in some cases to get the best contrast between the lunar dust simulant particles and the background. Water contact angle measurements were taken using a First Ten Angstroms (FTA) 1000B contact angle goniometer. Each measurement was conducted in triplicate with an 8 µl water droplet. Advancing and receding contact angle values were obtained using tilting axis measurements. Contact profilometry data was collected using a Bruker Dektak XT profilometer with a tip radius of 12.5 µm, a stylus force of 3 mg, a travel distance of 0.5 mm, and a scan duration of 60 s. Three scans at different locations were collected and averaged to determine surface roughness values.

Table 2. Laser Ablation Parameters.

Material	Wavelength, [nm]	Power, [W]	Frequency, [kHz]	Line Spacing, [µm] (mils)
Kapton® HN (Dupont™)	355	2.1	400	63.5 (2.5)
Teflon™ FEP	355	2.8	200	50.8 (2)
LCLR	355	1.2	400	50.8 (2)
Ti-6Al-4V	1064	12.2	400	63.5 (2.5)

Dust adhesion testing and estimation of characteristic forces

The lunar dust simulant, NU-LHT-1, designed by the United States Geological Survey (USGS), with a maximum particle size of 30 microns was used. This size is representative of the finer particles in lunar highland region that adhere to surfaces causing contamination issues. Small test coupons less than 10 mm in diameter were cut from each material. The samples were cleaned with isopropanol and dried before dust deposition. A mask was made to cover the sample surface to allow only a small circular window, ~ 8 mm in diameter, on the surface to be exposed to the dust. An approximate monolayer of dust was deposited on the sample by a previously developed aerosolization technique that lofted dust uniformly onto the surface [6]. The deposition was carried out under ambient conditions in the laboratory.

The particle contaminated surface was then subject to the dust adhesion testing system, which included an ultrasonic converter and horn (ultrasonic wand), the Sonics VCX 750 equipped with a 12.7 mm (0.5") diameter tip and an aerosol particle size spectrometer, the Topas GmbH LAP 322. The sample was attached on the tip of the ultrasonic wand and agitated to dislodge particles using a specified recipe to set the pulse period and amplitude. The maximum

displacement amplitude for this ultrasonic wand is 120 µm. Each sample was subjected to an initial brief run at the lowest amplitude setting of the ultrasonic wand system (approximate displacement of 24 µm) to remove any cohesively attached particles and any particles that exhibited an adhesion force with the surface that was equal to or less than the particle cohesion force of 0.52 KPa [7]. In the next step, the amplitude was ramped up in fixed time intervals (2 s) till the predetermined limit. Neglecting the hysteresis curve of the piezo and assuming a linear relation for this analysis, the approximate maximum displacement was 72 µm. The ultrasonic wand was not taken to the maximum power setting, i.e., maximum displacement, to prevent the sample from detaching from the ultrasonic wand tip surface. The particles detached during the process were detected by the aerosol particle size spectrometer. Optical microscopy images of the surfaces were taken after each experimental step to analyze the particles remaining adhered to the surface. The results provide a qualitative measure of the dust particle adhesion characteristics of the sample.

The displacement of the ultrasonic wand tip surface, Z, can be modeled by the equation:

$Z = A \sin(2\pi f t)$, where A is ½ the maximum amplitude (µm) of the ultrasonic wand, f is the ultrasonic wand frequency (Hz) and t is the time in seconds (s). For our system, f is constant at 20 KHz.

The maximum acceleration can be calculated by obtaining the second derivative of Z. By multiplying the mass of a particle with the maximum acceleration we can calculate the characteristic force on it at each amplitude setting. For example, if a spherical SiO_2 particle of diameter 4 µm remained adhered to a smooth material surface at the end of the experiment, considering its density to be 2320kg/m^3, its mass can be calculated to be 7.77e^{-2} ng. The characteristic force on it for different amplitude settings is shown in Table 3 below. For the particle to remain attached to the surface, the adhesion force must be greater than this characteristic force.

Table 3. Characteristic force calculations for a 4 µm spherical SiO_2 particle on the ultrasonic wand tip surface at different amplitude settings of the instrument.

% Max Amplitude	Amplitude [um]	Maximum acceleration [m/s^2]	Characteristic Force [nN]
20%	24	1.89E+05	14.69
40%	48	3.79E+05	29.46
60%	72	5.68E+05	44.16
80%	96	7.58E+05	58.93
100%	120	9.47E+05	73.62

These calculated forces are useful to provide context for the measurement technique, however this is a very simplified model using a spherical particle and does not reflect the full complexity

of the ultrasonic tip forces for a definitive assessment of the adhesive force of a surface. Therefore, the dust adhesion mitigating properties of one surface can be compared with another qualitatively by counting and measuring the size distribution of particles remaining adhered to the surface after a consistent testing sequence with the ultrasonic wand adhesion test.

Results and discussion

In each polymeric material selected, both the as-received control surface and the laser ablation patterned surface (Table 2) were tested for dust simulant adhesion properties. Due to experimental condition limitations, the FEP samples were tested for fewer steps. In the Ti alloy and the composite samples, only the patterned samples were tested as of the time of this reporting.

Surface modification of Kapton® HN through laser ablation patterning was characterized using optical and high-resolution SEM (Figure 2). Kapton® HN can readily absorb the 355 nm laser photons resulting in most of the excitation energy being utilized for photochemical ablation. This results in a relatively clean perimeter around the ablation lines (Figure 2a). Likewise, the morphology within the ablation lines is smooth and non-porous, features that have been observed when this material is ablation patterned using different ablation conditions (data not shown).

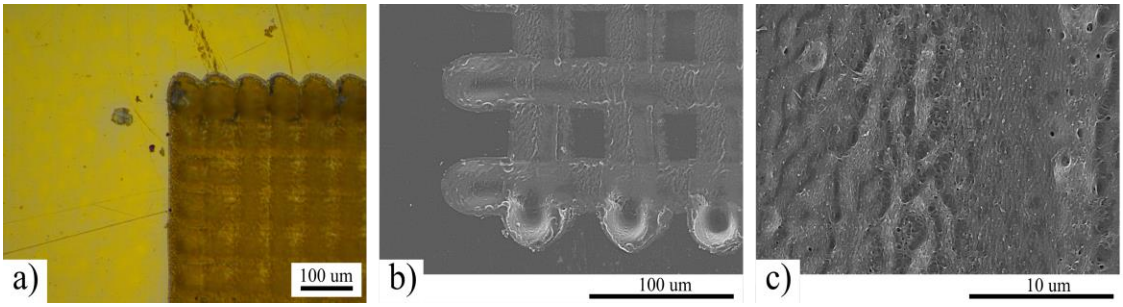

Figure 2. Optical (a) and scanning electron (b,c) micrographs of laser ablation patterned Kapton® HN surface.

Optical microscopy images of the as-received Kapton® HN film surface after lunar dust simulant deposition, the initial short run and then the full run are shown in the images below (Figure 3).

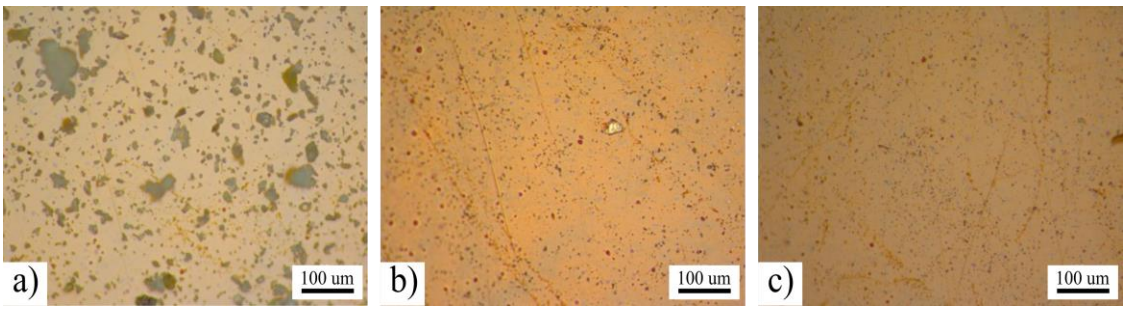

Figure 3. Optical microscopy images of the as-received Kapton® HN film surface at 20x magnification a) lunar dust simulant contaminated b) after initial run c) at the end of the dust adhesion test.

It is observed that while many of the larger particles were detached from the surface, a significant number of particles remain adhered.

The optical microscopy images at 20x magnification for the simulant contaminated laser ablation patterned Kapton® HN film surface after dust deposition, the initial short run and then the full run is shown in the Figure 4 below.

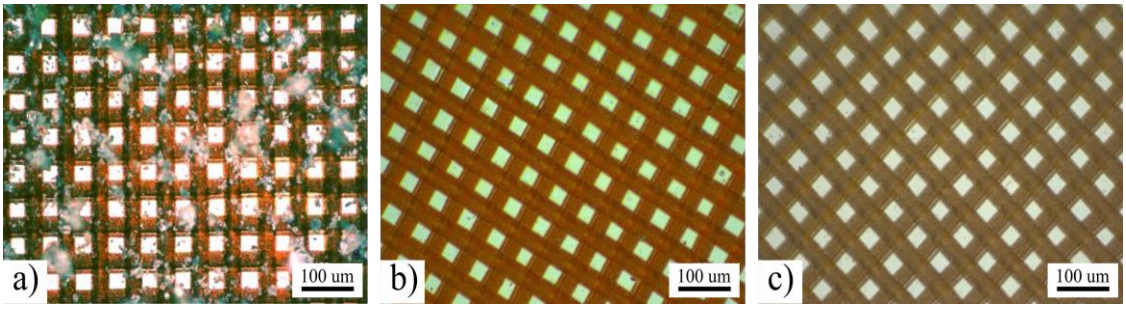

Figure 4. Optical microscopy images of the laser ablation patterned Kapton® HN film surface at 20x magnification a) lunar dust simulant contaminated b) after initial run c) at the end of the adhesion test.

The micrographs indicated that the laser patterned Kapton® HN had minimum adherence of lunar dust simulant. This result agrees with the counts registered by the optical particle counter, where more particles were detected after detaching from laser ablation patterned Kapton® HN compared to the as-received Kapton® HN surface.

HRSEM images were also collected on laser ablation patterned FEP surfaces (Figure 5). Streaking/splashing were observed around the ablation lines, indicating that a significant portion of the laser energy was transferred to photothermal ablation. Likewise, porous morphologies were observed extensively on the FEP surfaces. The observed granularity in surface structures and morphology may be related to the semi-crystallinity of FEP.

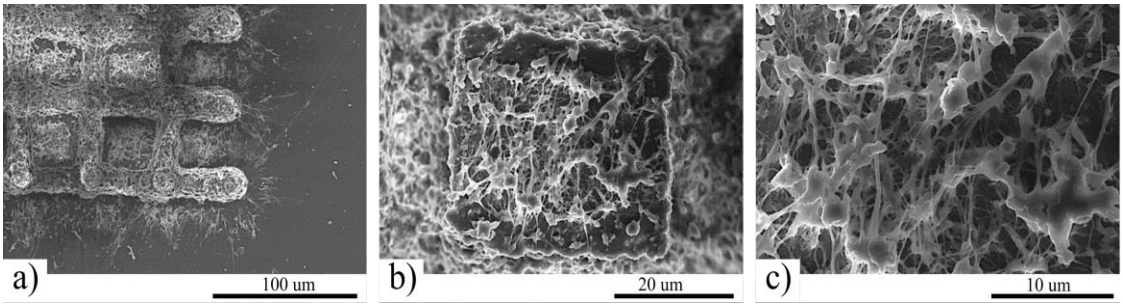

Figure 5. HRSEM micrographs collected on laser ablation patterned FEP using crosshatch pattern parameters from Table 2.

It was observed that, as with the Kapton® HN surfaces, laser ablation patterning improved the dust simulant adhesion performance of FEP relative to the pristine surface.

To enable evaluation of the influence laser ablation had on the dust simulant adhesion properties of titanium surfaces, the as-received material was polished using a lapping plate. Average roughness values, Ra, collected on the polished Ti-6Al-4V surfaces using contact profilometry were approximately 43±2 nm (Table 3). Laser ablation patterning of the metal surfaces using a picosecond laser provided a unique capability to impart a hierarchical surface topography into the sample in a single step. As a result of an interference pattern, a topography was generated on the surface perpendicular to the laser travel path. This process is called laser-induced periodic surface structures (LIPSS) and generates topographies with a periodicity approximately equal to the laser wavelength [8,9]. Combining the LIPSS topography (1 µm periodicity) with the direct-write crosshatch pattern (approximately 60 µm periodicity) resulted in the hierarchical topography observed through optical and SEM images for the Ti-6Al-4V surface (Figure 6a-e).

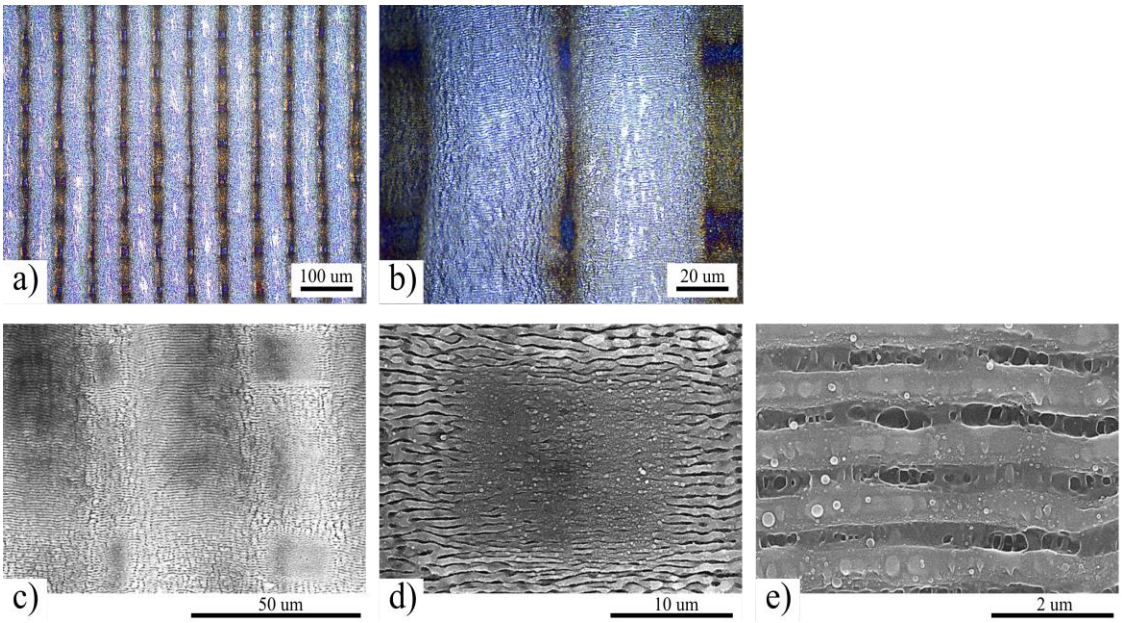

Figure 6. Image of Ti-6Al-4V samples at various stages of polishing. Optical (a and b) and scanning electron (c-e) micrographs collected on a laser ablation patterned Ti-6Al-4V surface.

With the Ti-6Al-4V samples, the laser ablation patterned surface showed greater dust adhesion mitigation relative to the pristine surface. The optical microscopy images at 20x magnification for the simulant contaminated Ti alloy surface with pattern #1 after dust deposition and the initial short run is shown in the Figure 7 below.

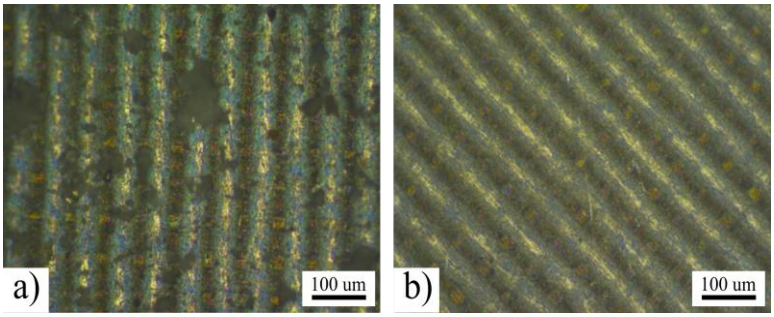

Figure 7. Optical microscopy images at 20x magnification of the laser ablated Ti-6AL-4V crosshatch pattern sample surfaces a) after dust deposition and b) the initial run.

Laser ablation patterning of the LCLR samples resulted in surfaces with the smoothest morphology within the ablation path of any of the materials evaluated here, based on empirical observations of microscopy images (Figure 8). This could arise from the highly cross-linked nature of the LCLR material as well as the absorption of this material at the lasing wavelength resulting in significant energy transfer to photochemical ablation mechanisms. The crosshatch pattern utilized for laser ablation conditions described in this work resulted in the generation of a square pillar array.

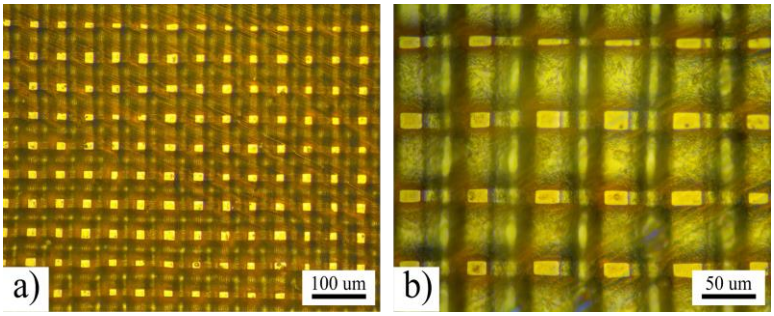

Figure 8. Optical microscopy images collected on laser ablation patterned LCLR surfaces.

The composite samples showed the greatest dust adhesion of all the samples tested during this experiment. Laser ablation patterning did show some level of observable dust mitigation at the end of the experiment but not with the same differentiation that was observed for the other substrates. The optical microscopy images at 20x magnification for the simulant contaminated laser ablated LCLR surface after dust simulant deposition and after the full run are shown in the images in Figure 9 below.

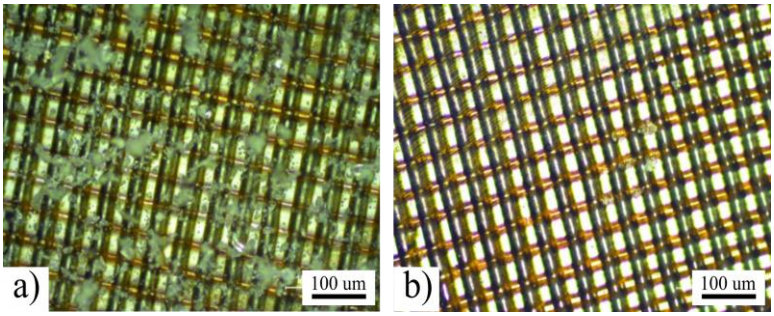

Figure 9. Optical microscopy images at 20x magnification of the LCLR-B crosshatch pattern composite sample surfaces a) after dust deposition and b) at the end of the adhesion test respectively.

Many factors influence the adhesion behavior of the dust particles on the surface, including the surface chemistry, topography, and mechanical properties of both the surface and the contaminating particles. Previously it has been found that lower energy surfaces generally show greater particle adhesion mitigation [10,11]. Water contact angle measurements were done to evaluate the surface energies and compare relative values with the dust adhesion data. Surfaces with a higher contact angle, i.e, lower surface energy, would likely exhibit lower dust adhesion. The results for pristine and laser ablation patterned Kapton® HN and Teflon™ FEP are plotted as shown in Table 4 below, where θ_A and θ_R are the advancing and receding water contact angles respectively:

Table 4. Surface Properties of Pristine and Laser Ablated Samples.

Material	Topography	θA [°]	θR [°]	Ra [µm]
Kapton® HN (Dupont™)	Pristine	78±3	58±5	0.041±0.011
	Laser Patterned	90±1	75±3	1.759±0.112
Teflon™ FEP	Pristine	106±7	95±1	0.022±0.005
	Laser Patterned	141±6	119±3	1.488±0.438
LCLR-B composite	Pristine	95±0.5	79±0.7	0.074±0.011
	Laser Patterned	81	66	1.541±0.158
Ti-6Al-4V	Pristine	86	73	0.043±0.002
	Laser Patterned	117±21	97±16	0.245±0.026

It is observed that laser ablated Kapton® HN had a much higher contact angle than the as-received pristine Kapton® HN surface, and in this case the increase in θ_A correlated with the improved lunar simulant adhesion mitigation performance. Similarly, for FEP, the patterned surface also had a higher θ_A and improved dust simulant adhesion performance relative to the as-received pristine surface. For LCLR-B composite, the laser patterned surface had lower θ_A than the pristine surface, however it had very good adhesion mitigation. In case of Ti-6Al-4V,

laser patterning also caused an increase in $\theta_{A,}$ and the surface had improved simulant adhesion mitigation performance.

Conclusion

Our present work was mainly qualitative in nature, to down-select suitable materials for evaluation on the RAC payload. The work was also done in a limited time with reduced access to the laboratory due to the pandemic. More research needs to be done to better understand the effects of various factors on dust adhesion including surface chemistry, surface topography, surface mechanical properties, and surface conductivity, among others. Further work is being planned to investigate these areas including computational modeling. In the future, when the results from the RAC payload experiment on the lunar surface are obtained, these results will be compared to those described in this work to ascertain the efficacy of Earth-based characterization and testing related to lunar dust adhesion mitigation.

Acknowledgements

The authors would like to acknowledge Dr. John Connell of the Advanced Materials and Processing Branch at NASA Langley Research Center. They would also like to acknowledge John Hopkins, Michael Oliver, Wade Hall, and John Lowe for substrate machining and topographical modification processes at NASA Langley Research Center. Funding was provided through NASA's Game Changing Development (GCD), Lunar Surface Innovation Initiative (LSII).

References

[1] Wagner, S. A. "The Apollo Experience Lessons Learned for Constellation Lunar Dust Management." *NASA Technical Publication TP-2006-213726. Washington, DC: National Aeronautics and Space Administration*, 2006.

[2] Dove, A., Devaud, G., Wang, X., Crowder, M., Lawitzke, A., and Haley, C. "Mitigation of Lunar Dust Adhesion by Surface Modification." *Planetary and Space Science*, Vol. 59, No. 14, 2011, pp. 1784–1790. https://doi.org/10.1016/j.pss.2010.12.001.

[3] Margiotta, D. V., Peters, W. C., Straka, S. A., Rodriguez, M., McKittrick, K. R., and Jones, C. B. The Lotus Coating for Space Exploration: A Dust Mitigation Tool. 2010.

[4] Calle, C. I., Buhler, C. R., Johansen, M. R., Hogue, M. D., and Snyder, S. J. "Active Dust Control and Mitigation Technology for Lunar and Martian Exploration." *Acta Astronautica*, Vol. 69, Nos. 11-12, 2011, pp. 1082–1088. https://doi.org/10.1016/j.actaastro.2011.06.010.

[5] Wohl, C., Belcher, M., Hopkins, J., and Connell, J. Topographical Modification of Materials for Lunar Dust Adhesion Mitigation. 2009.

[6] Wohl, C. J., Atkins, B. M., and Connell, J. W. *Method and Apparatus for the Quantification of Particulate Adhesion Forces on Various Substrates*. National Aeronautics; Space Administration, Langley Research Center, 2011.

[7] Colwell, J. E., Batiste, S., Horányi, M., Robertson, S., and Sture, S. "Lunar Surface: Dust Dynamics and Regolith Mechanics." *Reviews of Geophysics*, Vol. 45, No. 2, 2007. https://doi.org/10.1029/2005rg000184.

[8] Bonse, J., Höhm, S., Kirner, S., Rosenfeld, A., and Krüger, J. Laser-Induced Periodic Surface Structures (LIPSS) a Scientific Evergreen. 2016.

[9] Driel, H. M. van, Sipe, J. E., and Young, J. F. "Laser-Induced Periodic Surface Structure on Solids: A Universal Phenomenon." *Physical Review Letters*, Vol. 49, No. 26, 1982, pp. 1955–1958. https://doi.org/10.1103/physrevlett.49.1955.

[10] Wohl, C., Lin, Y., Belcher, M., Palmieri, F., Atkins, B., and Connell, J. Generation and Evaluation of Lunar Dust Adhesion Mitigating Materials. 2011.

[11] Wohl, C., Wiesner, V., King, G., Connell, J., and Miller, S. "Low Surface Energy Materials for Lunar Dust Adhesion Mitigation." *The Impact of Lunar Dust on Human Exploration*, Vol. 2141, 2020, p. 5014.